Journal of Medicinal Chemistry

Article

pubs.acs.org/jmc

Tailoring of Integrin Ligands: Probing the Charge Capability of the Metal Ion-Dependent Adhesion Site

Markus Bollinger,[†] Florian Manzenrieder,[†] Roman Kolb,[†] Alexander Bochen,[†] Stefanie Neubauer,[†] Luciana Marinelli,[‡] Vittorio Limongelli,[‡] Ettore Novellino,[‡] Georg Moessmer,[§] Reinhard Pell,[∥] Wolfgang Lindner,[∥] Joseph Fanous,[⊥] Amnon Hoffman,[⊥] and Horst Kessler*[,†,@]

[†]Institute for Advanced Study and Center of Integrated Protein Science, Department Chemie, Technische Universität München, Lichtenbergstrasse 4, 85747 Garching, Germany

[‡]Dipartimento di Chimica Farmaceutica e Tossicologica, Università di Napoli "Federico II", Via D. Montesano, 49-80131 Napoli, Italy

[§]Institut für Klinische Chemie und Pathobiochemie, Klinikum rechts der Isar, Technische Universität München, Ismaninger Strasse 22, 81675 München, Germany

[∥]Institute of Analytical Chemistry, University of Vienna, Währinger Strasse 38, A-1090 Vienna, Austria

[⊥]School of Pharmacy, Faculty of Medicine, The Hebrew University of Jerusalem, P.O. Box 12065, Jerusalem 91120, Israel

[@]Chemistry Department, Faculty of Science, King Abdulaziz University, P.O. Box 80203, Jeddah 21589, Saudi Arabia

Supporting Information

ABSTRACT: Intervention in integrin-mediated cell adhesion and integrin signaling pathways is an ongoing area of research in medicinal chemistry and drug development. One key element in integrin−ligand interaction is the coordination of the bivalent cation at the metal ion-dependent adhesion site (MIDAS) by a carboxylic acid function, a consistent feature of all integrin ligands. With the exception of the recently discovered hydroxamic acids, all bioisosteric attempts to replace the carboxylic acid of integrin ligands failed. We report that phosphinates as well as monomethyl phosphonates represent excellent isosters, when introduced into integrin antagonists for the platelet integrin αIIbβ3. The novel inhibitors exhibit in vitro and ex vivo activities in the low nanomolar range. Steric and charge requirements of the MIDAS region were unraveled, thus paving the way for an in silico prediction of ligand activity and in turn the rational design of the next generation of integrin antagonists.

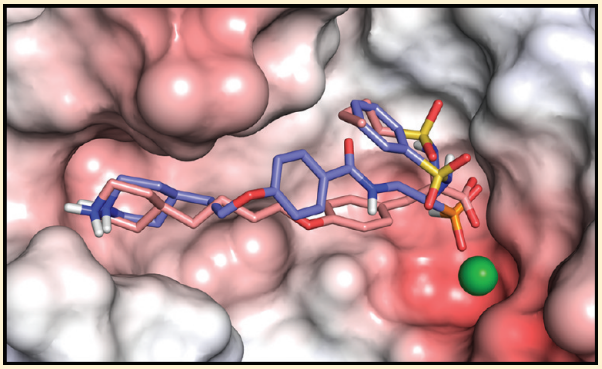

INTRODUCTION

Integrin signaling is profoundly implicated in numerous physiological processes, such as tissue remodeling or angiogenesis, as well as in important pathological disorders such as thrombosis, cancer, osteoporosis, and autoimmune diseases. Because of their biological relevance in many diseases, integrins represent highly important targets for medicinal chemistry.[1,2] From a structural point of view, integrins are heterodimers of a noncovalently linked α-subunit and a β-subunit. Each domain is composed of an extracellular domain, a single membrane-spanning helical domain, and a short cytoplasmic tail. The β-subunit contains a metal ion-dependent adhesion site (MIDAS) in the ligand binding domain.[3−5] Among the 24 known integrins, a number of them, known as the RGD-dependent integrins, recognize the tripeptide sequence arginine-glycine-aspartic acid (RGD) of extracellular matrix (ECM) proteins (e.g., fibronectin for α5β1, fibrinogen for platelet integrin αIIbβ3, and vitronectin for αvβ3 and other αv integrins) or other ligands, such as ADAMs, snake venoms, or viruses (FMD).[1,6,7] Constraining and mimicking RGD has successfully been used to develop thousands of integrin ligands, all containing an essential carboxylate moiety as a metal-coordinating group in the MIDAS. Recently, we found hydroxamic acids as a first potent isosteric replacement of the carboxylic group in integrins αvβ3 and α5β1.[8] The known tendency of phosphate groups to coordinate bivalent metal ions (calcium, manganese, or magnesium) prompted us to develop new phosphorus-containing integrin ligands with the aim of unraveling the steric and electrostatic requirements of the MIDAS region and obtaining significant new insights into the binding mode of integrins for further optimizing integrin ligands.

To date, extensive efforts have been made to discover and develop integrin antagonists for clinical applications. However, only for three integrins[9] (αIIbβ3, α4β1, and αLβ2), of the 24

Received: October 14, 2011
Published: December 19, 2011

   dx.doi.org/10.1021/jm2013826 | J. Med. Chem. 2012, 55, 871−882

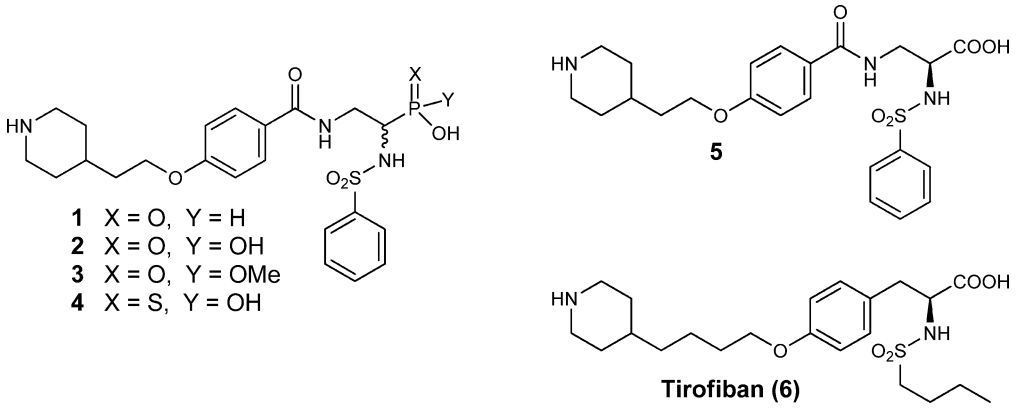

Figure 1. Bioisosteric replacement of the carboxylic MIDAS binding motif for the development of new αIIbβ3 integrin antagonists: phosphinic acid **1**, phosphonic acid **2**, monomethyl phosphonic acid **3**, thiophosphonic acid **4**, tirofiban analogue **5**, and tirofiban **6**.

Scheme 1. Synthesis of Integrin Ligands 1–4[a]

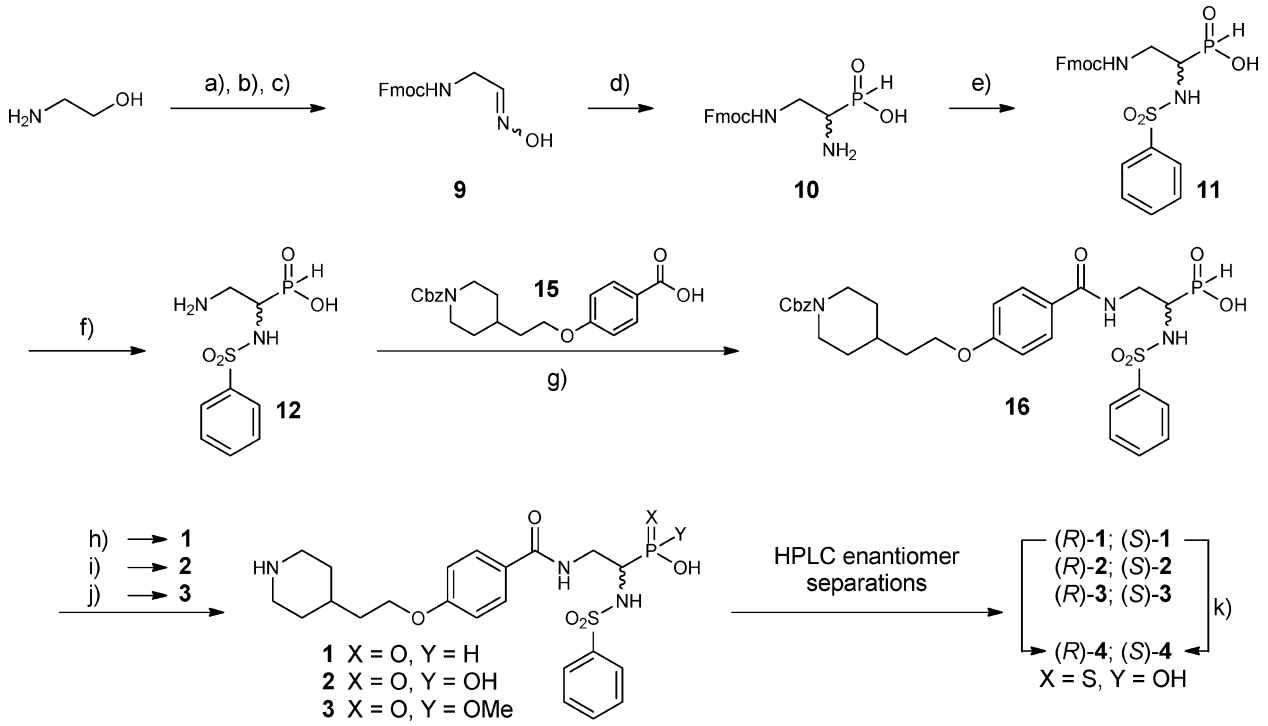

[a](a) Fmoc-Cl, 10% Na_2CO_3, room temperature (RT), 2 h; (b) IBX, DMSO, RT, 16 h; (c) $NH_2OH{\cdot}HCl$, DIEA, DCM, RT, 16 h; (d) anhydrous crystalline H_3PO_2, MeOH, reflux, 4 h; (e) $PhSO_2Cl$, 10% Na_2CO_3, dioxane, RT, 3 h; (f) 20% piperidine/DMF, RT, 2 h; (g) HATU, DIEA, DMF, RT, 16 h; (h) TFA/H_2O/TIPS, RT, 16 h; (i) (1) BSA, air, DCM, RT, 1 h; (2) TFA/H_2O/TIPS, 16 h; (j) (1) BSA, air, DCM, RT, 1 h; (2) EDC·HCl, DMAP, MeOH, RT, 1 h; (3) TFA/H_2O/TIPS, 16 h; (k) BSA, sulfur, DCM, RT, 1 h. All compounds were purified by RP-HPLC (for more details, see the Supporting Information).

known, have small molecular ligands been approved as drugs. Candidates for other integrins, such as $\alpha v\beta 3$, are in clinical phase III trials.[10] In contrast, significant advances have been made in targeting platelet integrin αIIbβ3.[9,11] In fact, the αIIbβ3 integrin inhibitor tirofiban[12] is being successfully used in acute antithrombotic therapy;[12−14] thus, inhibition of this receptor is now a validated way of inhibiting fibrinogen-dependent platelet aggregation.

In this work, integrin antagonists **1**–**4** (Figure 1) were developed on the basis of tirofiban analogue **5** (Figure 1) previously described by Duggan et al.[15] Compounds **1**–**4** allow us to explore the sensitivity of the MIDAS region for coordination of differently charged groups. Synthetic methods for obtaining the desired compounds **1**–**4** have been developed (Scheme 1). Enantiomers due to the chiral center in α-position of the phosphorus-containing group were resolved via chromatography on chiral columns and tested independently. The ability of the novel ligands to inhibit the binding of integrin αIIbβ3 to its corresponding ECM protein fibrinogen was tested in a competitive ELISA, and the efficacy of the most active compounds was proven in ex vivo experiments. To understand the dependency of the charge of the metal-coordinating group and the corresponding biological activities, we studied the protonation states of compounds **1**–**4** by means of extensive theoretical calculations and ^{31}P NMR titration experiments. The combination of ab initio calculations and molecular

dx.doi.org/10.1021/jm2013826 | J. Med. Chem. 2012, 55, 871–882

Table 1. Biological Evaluation of Activities of Ligands 1−6 on Integrin αIIbβ3

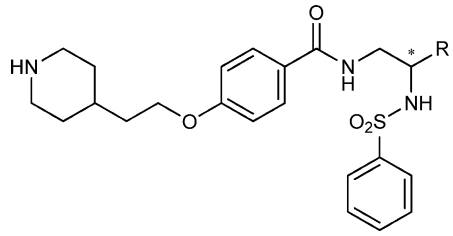

compd	R	IC_{50}[a] (nM) (αIIbβ3)	EC_{50}[b] (nM) (αIIbβ3)
(*R*)-**1**	PHOOH	1.2 ± 0.06	7.8 ± 0.9
(*S*)-**1**		6.3 ± 0.73	
(*R*)-**2**	$PO(OH)_2$	22.7 ± 2.7	276 ± 15.6
(*S*)-**2**		136 ± 10.7	
(*R*)-**3**	PO(OH)(OMe)	3.3 ± 0.4	40.8 ± 1.9
(*S*)-**3**		1154 ± 272	
(*R*)-**4**	$PS(OH)_2$	62.5 ± 6.0	
(*S*)-**4**		1322 ± 498	
(*S*)-**5**	COOH	0.81 ± 0.05	
(*R*)-**5**		4.4 ± 0.3	
6	tirofiban	0.95 ± 0.09	13.6 ± 3.3

[a] IC_{50} values were derived from a competitive ELISA using immobilized fibrinogen and soluble integrin αIIbβ3. [b] Effective concentrations (EC_{50}) of some key compounds for inhibition of platelet aggregation were derived from aggregation measurements using multiple-electrode aggregometry in hirudin-anticoagulated TRAP-6-activated blood.

docking simulations has defined the binding modes of the new ligands **1** and **2** identifying the molecular requisites for achieving a high inhibitory activity, and on the basis of these, a prediction of the activity of **3** and **4** was successfully executed.

CHEMISTRY

To prepare compounds **1**−**4**, two major fragments (**12** and **15**) were connected via an amide bond (Scheme 1). For the synthesis of **12**, commercially available 2-aminoethanol was Fmoc-protected followed by oxidation with IBX.[16,17] The corresponding aldehyde **8** was converted with hydroxylamine hydrochloride in DCM to oxime **9** in high yield.[18] Refluxing oxime **9** with anhydrous crystalline phosphinic acid in dry methanol resulted in racemic phosphinate intermediate **10**,[18,19] which was sulfonylated upon treatment with phenylsulfonyl chloride in aqueous Na_2CO_3 to provide Fmoc-protected derivative **11**. Fmoc deprotection and purification by reverse-phase high-performance liquid chromatography (RP-HPLC) afforded fragment **12** as a racemic mixture.

The second fragment containing the arginine mimic as a piperidine moiety had already been described by Duggan et al.[15] Herein, Cbz protection was used instead of the more acid labile Boc group, to avoid any deprotection of the secondary amine during synthesis. Furthermore, during purification of **13**, the Cbz group allows UV detection. 2-[*N*-(Benzyloxycarbonyl)-piperidin-4-yl]ethanol (**13**) was coupled to methyl-4-hydroxybenzoate via Mitsunobu reaction with tributylphosphine and 1,1′-(azodicarbonyl)dipiperidine.[20,21] Saponification of methyl ester **14** gave benzoic acid derivative **15**. Activation of **15** by use of *O*-(7-azabenzotriazol-1-yl)-*N*,*N*,*N*′,*N*′-tetramethyluronium hexafluorophosphate (HATU) and subsequent condensation with **12** gave Cbz-protected precursor **16**.

Deprotection of **16** with trifluoroacetic acid yielded molecular probe **1**, while the conversion of phosphinic acid **16** to the bis(trimethylsilyl)phosphonite intermediate, which was oxidized by atmospheric oxygen, afforded after Cbz deprotection phosphonic acid ligand **2** in high yield. When this process was applied to **1** and an excess of sulfur was added, thiophosphonic acid **4** was obtained. Furthermore, Cbz-protected phosphonic acid **2** undergoes rapid monoesterification at room temperature in the presence of *N*-[3-(dimethylamino)propyl]-*N*′-ethylcarbodiimide (EDC) and 2 equiv of 4-dimethylaminopyridine (DMAP) in dry methanol. Without DMAP, the reaction results in exclusive formation of the dimethyl ester and no desired product **3** is observed.

We decided to synthesize all molecular probes as racemic mixtures, as "libraries of enantiomers". However, for a more detailed biological evaluation, it was necessary to determine the activity of the optically pure compounds.

Enantiomer separation was successfully performed on quinine-based chiral zwitterionic ion-exchange-type stationary phases developed by Hoffmann et al.[22] Here, a sulfonic acid derivative of quinine served as a zwitterionic chiral selector.[23] The concept of the resolution of the racemic ampholytes, as compounds **1**−**3** can be classified, is based on a simultaneous ion pair formation of the zwitterionic chiral selector motif of the chiral stationary phase with the individual enantiomers of the analytes. These two diastereomerically behaving selector−(*R*)-enantiomer and selector−(*S*)-enantiomer associates are the basis for the enantiomer separations.[22] The preference and magnitude of molecular recognition and chiral discrimination are based on the stereochemical properties of the chiral selector and the ampholytes that include additional intermolecular interaction sites like hydrogen bonding and π−π interactions that determine the overall chromatographic enantioselectivity and elution order.

For *N*-acyl-protected amino acid-type analytes with known absolute configurations, we formulated a general model of intermolecular interactions and chromatographic elution order that correlates with the absolute configuration of the α-carbon of an α-amino acid.[24,25] Accordingly, we assigned the stereocenter of compounds **1**−**3**, taking into account the isosteric behavior of the analytes and the Cahn−Ingold−Prelog

dx.doi.org/10.1021/jm2013826 | J. Med. Chem. 2012, 55, 871−882

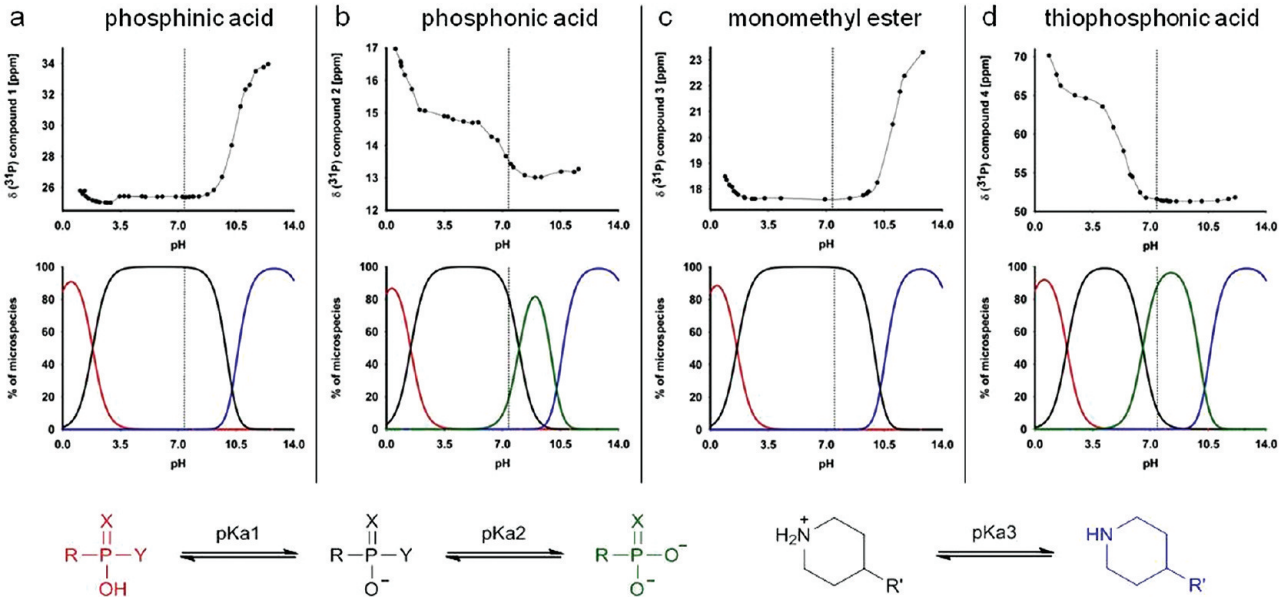

Figure 2. Assessing the protonation state of the molecular probes. Comparison of ^{31}P NMR titration curves (top) and computed microspecies distributions (middle) for molecular probes **1**–**4** (a–d, respectively). The physiological pH of 7.2 is shown as a dotted line to highlight the presence of either a single protonation state [horizontal line for **1** (a), **3** (c), and **4** (d)] or two protonation states [descending line for **2** (b)]. In the calculated microspecies distribution (bottom), structures of the most dominant protonation states are shown. The dotted line and the intersection with the presentation of microspecies represent the protonation states at the physiological pH of 7.2.

(CIP) convention (for more details, see the Supporting Information).

RESULTS

In Vitro Inhibition of Integrin αIIbβ3. To validate the inhibition properties of the compounds against αIIbβ3, a competitive ELISA (αIIbβ3 fibrinogen assay) was performed using soluble integrin αIIbβ3 and the immobilized natural ligand fibrinogen.[26,27] The clinically used αIIbβ3 inhibitor tirofiban was used as an internal control (Table 1, IC_{50}).

Carboxylic acid (*S*)-**5** is similar in potency to tirofiban (**6**), whereas the (*R*)-configuration is 6 times less active (0.8 nM vs 4.4 nM). Isosteric replacement of the carboxylic acid with a phosphinic acid results in retained activity depending on its relative configuration [1.2 nM for (*R*)-**1** and 6.3 nM for (*S*)-**1**]. However, the phosphonic acid derivatives **2** are 20 times less active [22.7 nM for (*R*)-**2** and 136 nM for (*S*)-**2**] than phosphinic acid **1**, clearly indicating that additional negative charge is not well tolerated in the MIDAS. Being aware that phosphonic acid **2** might exist in several different protonation states at the given pH, we used thiophosphonic acid **4** as a molecular probe existing only in the double-negative protonation state (Figure 2). The higher IC_{50} of **4** [62.5 nM for (*R*)-**4** and 1322 nM for the less favored (*S*)-**4** enantiomer] indicates that the additional charge in phosphonates and thiophosphonates reduces the binding affinity for the MIDAS. To further prove and underline this concept, we evaluated monomethyl ester **3** of phosphonic acid **2**, resulting in the elimination of the additional negative charge. The (*R*)-**3** phosphonic methyl ester regains nearly all of the activity (3.3 nM) compared to the phosphinic acid (*R*)-**1**, whereas the (*S*)-**3** methyl ester is far less potent (1154 nM). This could indicate a steric hindrance by the methyl group pointing toward the binding pocket. Similar indications were obtained from the docking calculations (for more details, see the Supporting Information).

Platelet Aggregation in Whole Blood. In an attempt to compare the potencies of binding of various compounds to isolated platelet integrin αIIbβ3 (IC_{50}) with their predicted inhibitory potency for the complex biological process of platelet aggregation, the effects of synthetic ligands (*R*)-**1**, (*R*)-**2**, (*R*)-**3**, and tirofiban on ex vivo platelet aggregation were assessed using impedance-based platelet aggregometry[28,29] in hirudin-anticoagulated TRAP-6-activated whole blood (Table 1, EC_{50}).

Phosphinic acid (*R*)-**1** was found to behave like tirofiban in terms of platelet aggregation inhibition, whereas phosphonic acid derivative (*R*)-**2** was ~20 times less potent. Phosphonic methyl ester (*R*)-**3** showed intermediate efficacy. There is a very good correlation between the inhibitory potencies of compounds in the ELISA (IC_{50}) and their inhibitory potencies in the platelet aggregation assay (EC_{50}).

In Vitro Permeability Study. We have tested pharmacokinetic properties (including disposition and membrane permeability) of ligands **1**–**3** and tirofiban (**6**) by evaluating their permeability properties with an enterocyte monolayer derived from human colonic carcinoma cells (Caco-2 model).[30] This model is commonly used to predict the degree of intestinal permeability of therapeutic compounds as well as to gain a certain indication regarding their likelihood of penetrating the brain. The results could not differentiate between the permeability properties of the four compounds in cases where all of them exhibit poor permeability properties ($P_{app} < 1 \times 10^{-8}$ cm/s). It should be noted that the permeability of mannitol (positive control) used in this study was 2.4×10^{-6} cm/s. The permeability mechanism of mannitol is paracellular, using the pores between the cells (tight junctions), with no transcellular component. The fact that all of the tested tirofiban analogues had significantly lower permeability values indicates that the charged moiety of these analogues (at physiological pH, 7.2) restricted the paracellular transport properties in an effective manner. However, to validate this argument, we prepared the corresponding dimethyl ester of **2** [inactive in the

dx.doi.org/10.1021/jm2013826 | J. Med. Chem. 2012, 55, 871–882

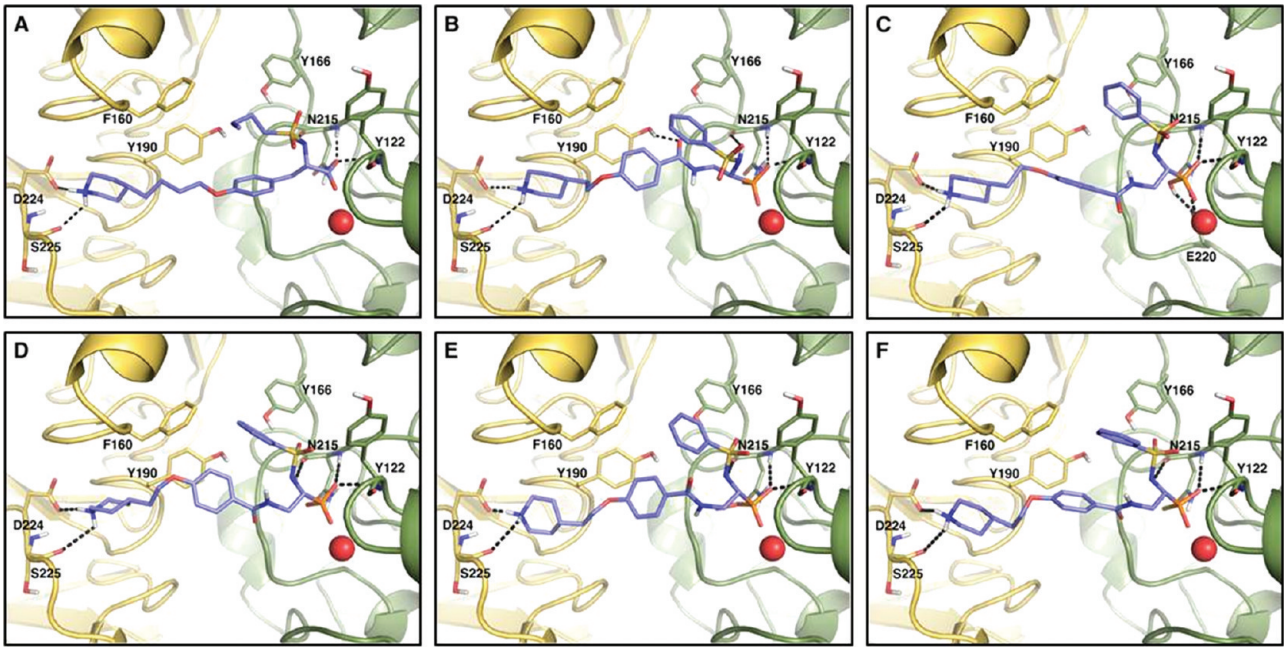

Figure 3. Modes of binding of tirofiban (A), (*R*)-**1** (B), (*R*)-**2** in the overall neutral form (C) and in the overall anionic form (D), (*R*)-**3** (E), and (*R*)-**4** (F). The αIIb domain is displayed as a yellow cartoon, while the β3 domain is colored green. The interacting residues and the ligands are shown as licorice, while the magnesium ion is represented as a red sphere. For the sake of clarity, only the polar hydrogens are displayed. The stereoview version of each complex is provided in Figure S3 of the Supporting Information.

αIIbβ3 fibrinogen assay (data not shown] and tested its permeability. Unfortunately, this compound also exhibited poor permeability.

Assessment of the Protonation State of 1−4. To elucidate the molecular properties responsible for the different activity profiles of the investigated compounds (Table 1) and the mechanism of recognition between the inhibitors and the αIIbβ3 integrin receptor (see the docking section), we conducted an extensive computational study. First, the protonation states of compounds **1**−**4** were computed for each compound, and the distribution of microspecies between pH 0 and 14 was calculated with the Marvin Sketch package. The results were validated via titration experiments monitored by ^{31}P NMR chemical shifts that are very sensitive to ionization state[31−35] (Figure 2; for more details, see the Supporting Information).

While **1** and **3** are characterized by two pK_a values, corresponding to the acidities of the phosphorus acid moiety (pK_{a1}) and the piperidinium group (pK_{a3}), for **2** and **4** a total of three pK_a values are found [phosphonic and thiophosphonic acid (pK_{a1} and pK_{a2}, respectively) and piperidinium group (pK_{a3})]. The experimental as well as the calculated (in parentheses) pK_a values show that at the physiological pH of 7.2 all piperidine moieties are protonated with pK_{a3} values of 10.44 (10.48) for **1**, 10.06 (10.48) for **2**, 11.02 (10.57) for **3**, and 12.03 (10.58) for **4**. Furthermore, the first acid functionality of the phosphorus unit (pK_{a1}) of all compounds **1**−**4** is present in the completely deprotonated form at pH 7.2 with pK_{a1} values of greater than 1.56 (1.90) for **1**, 1.01 (1.63) for **2**, 1.13 (1.63) for **3**, and 1.27 (1.94) for **4**. All in all, we found that the experimental NMR results fully corroborate the trends in the computational calculations.

At the physiological pH of 7.2, the piperidine moiety (pK_{a3}) of **1** is protonated and the phosphinate group (pK_{a1}) is fully deprotonated (Figure 2a). For **2**, two microspecies can be found at physiological pH, both having a protonated piperidine unit; however, in one case, the phosphonic acid is monoanionic (~86% in silico and 63% in vitro), and in the other case, it is in the dianionic form (~14% in silico and 37% in vitro) (Figure 2b). To further investigate the effect of the charge of the different substituents on the phosphorus atom, two more molecular probes, **3** and **4**, were studied. In particular, the thiophosphonate group of compound **4**, like the phosphonate group of **2**, coexists at neutral pH as mono- and dianionic species, but a shift toward the dianionic form (~82% in silico and 99% in vitro) was observed (Figure 2d). The in vitro measurements showed that the second acid functionality (pK_{a2}) of compounds **2** and **4** is more acidic than calculated. For **2** a pK_{a2} of 6.97 (7.99) and for **4** a pK_{a2} of 5.27 (6.53) can be extracted from the obtained data points. Compound **3**, like **1**, possesses only one single microspecies (Figure 2c).

Molecular Docking and Electrostatic Potential Calculations of 1−4. Compounds **1**−**4** were docked into the αIIbβ3 RGD binding site with the aid of AutoDock version 4.0.[36,37] Both enantiomers were studied. Results of the (*S*)-enantiomers are reported in the Supporting Information along with an explanation of the lower inhibitory potency observed for (*S*)-**1**, (*S*)-**2**, and (*S*)-**3** with respect to those of the corresponding (*R*)-enantiomers.

As for (*R*)-**1**, in accordance with the protonation state assessment (Figure 2a), only the neutral ligand form (piperidine moiety protonated, phosphinate deprotonated) was used for docking simulations. As a result, a binding mode highly similar to that of tirofiban was observed (Figure 3A,B and Figure S2 of the Supporting Information). In fact, the phosphinate group coordinates the magnesium ion occupying in the MIDAS the same region that hosts the carboxylate group of tirofiban. In particular, one of the oxygen atoms coordinates the metal, while the other one engages two H-bonds with the backbone NH groups of (β3)-Asn215 and (β3)-Tyr122, like

dx.doi.org/10.1021/jm2013826 | J. Med. Chem. 2012, 55, 871−882

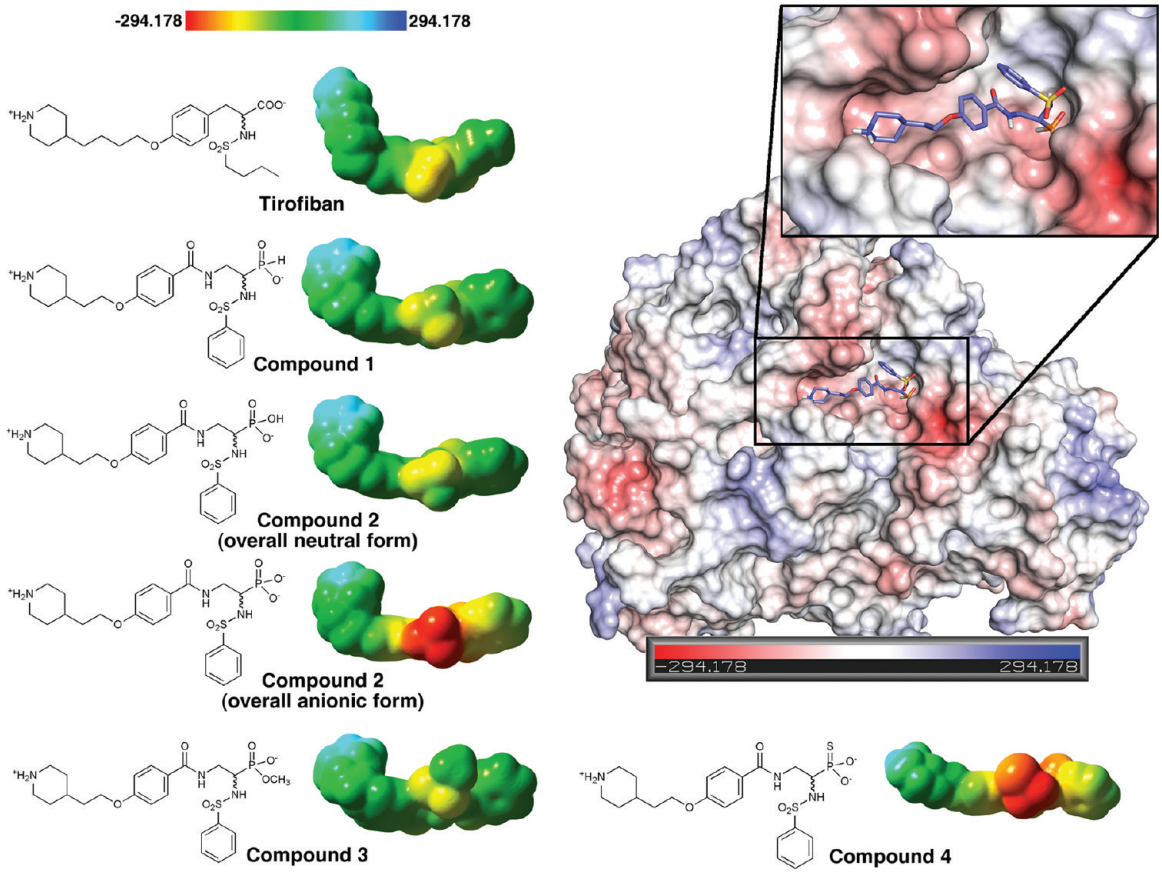

Figure 4. Electrostatic potential mapped onto the molecular surface of tirofiban, **1**, **2** in the overall neutral form and in the anionic form, **3**, and **4**. At the top right, the electrostatic surface of the integrin αIIbβ3 binding site complexed with compound (*R*)-**1** is shown. Both for ligands and for the protein, the scale of the electrostatic potential ranges from −294.178 (red) to 294.178 (blue) k_bT/e_c.

tirofiban in αIIbβ3 and Cilengetide in αvβ3 [Protein Data Bank (PDB) entries 2vdm and 1L5G]. The benzenesulfonamide moiety forms H-bonds with the (β3)-Asn215 backbone CO group, while the phenyl ring occupies the aromatic pocket formed by (αIIb)-Phe160, (αIIb)-Tyr190, and (β3)-Tyr166. The aromatic ring of the *p*-hydroxybenzoate scaffold is close enough to form a $\pi-\pi$ interaction with (αIIb)-Tyr190, the hydroxyl group of which is involved in an H-bond interaction with the inhibitor amide CO group. This allows the piperidine moiety to point toward the αIIb subunit, where the protonated nitrogen group makes a salt bridge interaction with the (αIIb)-Asp224 side chain and an H-bond with the (αIIb)-Ser225 backbone CO group. All these favorable interactions are certainly responsible for the low nanomolar activity of (*R*)-**1** toward the αIIbβ3 receptor.

Because phosphonic acid **2** is present at the physiological pH of 7.2 both in the monoanionic form and in the dianionic form (Figure 2b), docking calculations for (*R*)-**2** were performed for both protonation states, and the results showed a binding conformation similar to that of tirofiban and (*R*)-**1** (Figure 3C,D). This suggests that although the phosphonic group is bulkier than the phosphinate moiety, it can fit in the MIDAS region. Nevertheless, because (*R*)-**2** shows reduced activity compared to that of (*R*)-**1** (Table 1), reasons different from the steric hindrance should be responsible for the experimentally observed lower activity. In this regard, it has to be clarified that all docking algorithms, either based on classical force fields[38] or based on empirical free energy scoring functions[39] or knowledge-based scoring functions,[40] cannot accurately predict properties like the exact metal coordination geometry or particular charge effects. Thus, to overcome this limitation and to shed light on the different activity profiles of (*R*)-**1** and (*R*)-**2**, more accurate computational techniques must be used. Recent progress made in the force field parametrization of bivalent ions[41] and some theoretical studies on a Mg^{2+} protein[42,43] would suggest the use of molecular dynamics-based approaches to sample more accurately the specific ligand−protein interaction of each complex. Another possibility might be to perform QM/MM calculations to accurately describe the ligand−protein interaction at the binding site. Unfortunately, both these approaches are computationally time intensive and are useful for the study of only a few compounds. To perform calculations on most of the ligands of the series in a reasonable computational time, we decided to conduct quantum mechanical calculations only on the ligands, thus elucidating their different electrostatic potential profiles.

Quantum mechanical calculations revealed that (*R*)-**1** has an electrostatic potential profile highly similar to that of tirofiban, particularly with regard to the metal-coordinating group, while (*R*)-**2** is similar to tirofiban only in its neutral form (Figure 4). In fact, with regard to (*R*)-**2**, the electrostatic potential of the phosphonate group in the dianionic form, existing at physiological pH, is highly negative. Indeed, if on one hand this improves the coordination of the metal ion, on the other hand, it causes electrostatic repulsion effects with the surrounding atoms in the MIDAS such as the backbone CO groups of (β3)-Asn215 and (β3)-Asp217 or the (β3)-Glu220 side chain (Figures 3D and 4). Thus, our computational study

dx.doi.org/10.1021/jm2013826 | *J. Med. Chem.* 2012, 55, 871−882

of (*R*)-**1** and (*R*)-**2** suggests that electrostatic properties, more than steric features, are the crucial factors for the different activities of the two compounds.

Also in the case of (*R*)-**3** and (*R*)-**4**, it was not possible to predict the αIIbβ3 activities solely on the basis of the docking calculations (see Figure 3E,F for the predicted binding modes and the Supporting Information for further details about docking). As shown in Figure 4, the electrostatic potential profile calculated for (*R*)-**3** is highly similar to those of tirofiban and (*R*)-**1**, while compound (*R*)-**4**, like (*R*)-**2**, has a highly negative potential localized on the thiophosphonate group (dianionic form). Those results are in perfect line with the ELISA data reported in Table 1. In fact, (*R*)-**4** possesses a reduced activity because of the preponderance (~82% in silico and 99% in vitro) of its dianionic form, which has the less favorable electrostatic profile for its interaction with αIIbβ3. Accordingly, (*R*)-**3** has an electrostatic potential profile and an activity comparable to those of (*R*)-**1**.

DISCUSSION

The strong binding affinity of phosphorus ligands for bivalent metal ions stimulated us to investigate those groups as pharmacophores for binding to the MIDAS region of integrins. As a proof of principle, we investigated analogues of αIIbβ3 integrin inhibitor **5**, previously described by Duggan et al.,[15] which is structurally related to the drug tirofiban (**6**) and exhibits a similar binding affinity. The essential carboxyl group of **5** was modified by different phosphorus-containing groups. We found that phosphinate groups as well as a phosphonate monomethyl ester are suitable isosteres for the carboxyl group in integrin ligands while phosphonate and thiophosphonate groups could not be used for this purpose. Docking of ligands **1**−**4** in the αIIbβ3 receptor did not reveal substantial differences with respect to the tirofiban binding mode (Figure 3 and Figure S2 of the Supporting Information), thus excluding steric effects as a reason for different binding potencies. On the basis of ab initio studies, the high affinity of phosphinate **1** and phosphonate monomethyl ester **3** can be attributed to the lower negative charge of the ligand metal binding groups, if compared to those of **2** and **4** (Figure 4). The differences in charges among compounds **1** and **4** have been investigated both by theoretical calculations and by ^{31}P NMR measurements. In phosphonate **2** and thiophosphonate **4** at neutral pH, there are considerable amounts of dianionic species in the equilibrium (Figure 2). Obviously, the high negative charge is not tolerated by the MIDAS region, which is already negatively charged (Figure 4).

The dominating charge effect is accompanied by second-order steric effects induced by substituents in α-position to the phosphorus atom expressed in the different acceptance of stereoisomers. Synthesis and the biological assays of the pure (*R*)- and (*S*)-stereoisomers of **5** reveal that the (*R*)-enantiomer is ~5 times less active than the (*S*)-enantiomer. The same general trend was found for compounds **1**−**4**, bearing in mind the fact that according to the CIP rules the notation in the phosphorus compounds is reversed (Table 1). Molecular docking revealed that in the case of compounds **1**−**4**, although the (*S*)-enantiomers are also able to bind the receptor, they lose a number of favorable interactions within the binding pocket, particularly in the case of phosphonic compounds (*S*)-**2** and (*S*)-**3** (see the Supporting Information for details).

In the biological evaluation of the new αIIbβ3 antagonists, we have shown that the in vitro binding affinity fully correlates with the ex vivo prevention of platelet aggregation measured by multiple-electrode aggregometry in hirudin-anticoagulated TRAP-6-activated blood. Both assays yield the same order of activities for all tested compounds. Approximately 10-fold higher EC_{50} values are required compared to inhibition of binding of integrin to fibrinogen (Table 1, IC_{50}).

The pharmacotherapeutic activity of tirofiban is provided following intravenous administration and is confined to the systemic blood circulation. The results of the permeability studies can be regarded as an indication that the new ligands will also be restricted to the central compartment. Thus, once administered by a parenteral route, the molecules will be distributed within the central compartment where they produce their antiplatelet aggregation activity. In case the novel analogues will be further developed for clinical use (e.g., for molecular imaging), the restricted distribution predicted for these analogues ensures minimal side effects that could be derived by interaction with peripheral tissues, including the central nervous system. Thus, the poor membrane permeability contributes to the safety profile of these analogues. Pharmacokinetically wise, the polar moieties of these analogues at the physiological pH of 7.2 did not allow passive diffusion across the biological membrane, like enterocytes. It also inhibited the transport via the tight junctions pores as evidenced by the significantly lower permeability compared to that of mannitol.

In summary, we here report a successful case of drug design on the αIIbβ3 integrin that allowed us to identify the molecular and electrostatic requisites for achieving strong αIIbβ3 inhibition. In particular, we have found that even a space-demanding group such as methyl phosphonate (*R*)-**3** can bind to the αIIbβ3 MIDAS without strongly affecting the activity. We have found that highly negatively charged metal-coordinating groups are not well tolerated in the αIIbβ3 MIDAS. All these findings, on one hand, are extremely useful for an easy and quick tuning of both the steric and electrostatic features of αIIbβ3 inhibitors; on the other hand, they demonstrate that docking calculations together with more rigorous computational procedures, such as ab initio studies, can be successfully used in rational design of new inhibitors active on integrin receptors different from αIIbβ3.

The modification of the carboxylate group into a phosphinate or a phosphonate monomethyl ester yields an attractive new way of optimizing integrin ligands. The successful design of non-carboxylate-containing ligands as integrin antagonists surely opens a new era in the design and finding of novel integrin ligands.

EXPERIMENTAL SECTION

All technical solvents were distilled prior to use. Dry solvents were purchased from Aldrich, Fluka, or Merck. Reactions sensitive to oxygen or water were performed in flame-dried reaction vessels under an argon atmosphere (99.996%). Fmoc-protected amino acids and coupling reagents were purchased from Novabiochem (Schwalbach, Germany), Iris Biotech GmbH (Marktredwitz, Germany), and Medalchemy (Alicante, Spain). All other chemicals and organic solvents were purchased from commercial suppliers at the highest purity available and used without further purification.

TLC monitoring was performed on Merck DC silica gel plates (60 F-254 on aluminum foil). Spots were detected by UV absorption at 254 nm and/or by staining with a 5% solution of ninhydrine in ethanol or mostain [6.25 g of phosphomolybdic acid, 2.5 g of cerium(IV) sulfate, and 15 mL of sulfuric acid in 235 mL of water] or potassium permanganate (5% in 1 N aqueous NaOH).

dx.doi.org/10.1021/jm2013826 | J. Med. Chem. 2012, 55, 871−882

Flash column chromatography was performed using silica gel 60 (40−63 μm) from Merck at a pressure of 1−1.5 atm.

Analytical HPLC was performed using Amersham Pharmacia Biotech Äkta Basic 10F equipment, with a P-900 pump system, a reversed-phase YMC-ODS-A C_{18} column (12 nm pore size, 5 μm particle size, 250 mm × 4.6 mm), and UV detection (UV-900; 220 and 254 nm). The system was run at a flow rate of 1.0 mL/min over 30 min using H_2O (0.1% TFA) and MeCN (0.1% TFA) as solvents.

Semipreparative HPLC was performed using Waters equipment: System Breeze; pump system 1525, UV detector 2487 dual (220 and 254 nm); Driver Software Breeze version 3.20; column material, YMC-ODS-A C_{18} (12 nm pore size, 5 μm particle size, 250 mm × 20 mm), YMC-ODS-AQ C_{18} (12 nm pore size, 5 μm particle size, 250 mm × 20 mm), or YMCbasic (proprietary, 5 μm particle size, 250 mm × 20 mm).

HPLC−ESI-MS analyses were performed on a Hewlett-Packard Series HP 1100 system with a Finnigan LCQ mass spectrometer using a YMC-Hydrosphere C_{18} column (12 nm pore size, 3 μm particle size, 125 mm × 2.1 mm) or a YMC-Octyl C_8 column (20 nm pore size, 5 μm particle size, 250 mm × 2.1 mm). The system uses H_2O (0.1% formic acid) and MeCN (0.1% formic acid) as eluents.

High-resolution mass spectrometry was conducted on a Thermo Finnigan LTQ-FT (ESI-ICR) spectrometer.

^{1}H NMR, ^{13}C NMR, and ^{31}P NMR spectra were recorded at 295 K on 500 MHz Bruker DMX, 360 MHz Bruker AV, and a 250 MHz Bruker AV spectrometers, respectively (Bruker, Karlsruhe, Germany). Chemical shifts (δ) are given in parts per million. The following solvent peaks were used as internal standards: DMSO-d_5, 2.50 ppm (^{1}H NMR) and 39.52 ppm (^{13}C NMR); $CHCl_3$, 7.26 ppm (^{1}H NMR) and 77.16 ppm (^{13}C NMR); MeOH-d_3, 3.31 ppm (^{1}H NMR) and 49.00 ppm (^{13}C NMR).[44] With MeOH-d_3 as the solvent, standard pulse sequences provided by Bruker were used to eliminate the solvent peak (watergate, P3919GP; presaturation, ZGPR). For ^{31}P NMR spectra, 85% phosphoric acid was used as an external standard.

Duggan ligand (*S*)-**5** was synthesized according to literature procedures,[15] starting from N^{α}-Fmoc-L-2,3-diaminopropionic acid. Synthesis of the corresponding (*R*)-enantiomer was conducted as described here, starting from N^{α}-Boc-N^{β}-Fmoc-D-2,3-diaminopropionic acid. Standard peptide coupling techniques were employed.

All yields are not optimized. The analytical data of compounds **7**−**18** are listed in the Supporting Information. All tested compounds were ≥95% pure as determined by RP-HPLC-(MS).

1-(Phenylsulfonamido)-2-{4-[2-(piperidin-4-yl)ethoxy]-benzamido}ethylphosphinic Acid (1). A mixture of TFA, TIPS, and water [5 mL, 95:2.5:2.5 (v/v/v) TFA/TIPS/H_2O] was added to **16** (36.0 mg, 0.057 mmol) and the mixture stirred at room temperature (RT) for 16 h. Purification by semi-preparative RP-HPLC and lyophilization gave **1** (23.5 mg, 0.047 mmol, 83%) as a white solid: ^{1}H NMR (500 MHz, MeOH-d_3, RT) δ 8.53 (br s, 1 H), 8.24 (br s, 1 H), 8.10 (t, ^3J = 5.0 Hz, 1 H), 7.83 (d, ^3J = 7.6 Hz, 2 H), 7.66 (d, ^3J = 9.0 Hz, 2 H), 7.42 (t, ^3J = 7.3 Hz, 1 H), 7.37 (t, ^3J = 7.5 Hz, 2 H), 6.93 (d, ^3J = 9.0 Hz, 2 H), 6.83 (d, ^1J = 531.3 Hz, 1 H), 4.11 (t, ^3J = 6.2 Hz, 2 H), 3.66−3.48 (m, 3 H), 3.43−3.34 (m, 2 H), 3.07−2.87 (m, 2 H), 2.11−1.94 (m, 2 H), 1.96−1.84 (m, 1 H), 1.80 (dt, ^3J = 6.3 Hz, ^3J = 6.3 Hz, 2 H), 1.46 (dt, ^3J = 14.9 Hz, ^3J = 3.9 Hz, 2 H); ^{13}C NMR (126 MHz, MeOH-d_3, RT) δ 169.9, 163.2, 142.6, 133.6, 130.4, 130.2, 128.0, 127.5, 115.2, 66.6, 54.9 (d, $^1J_{PC}$ = 99 Hz), 45.5, 39.4 (d, $^2J_{PC}$ = 5 Hz), 36.2, 32.4, 30.1; ^{31}P NMR (101 MHz, D_2O/H_2O, RT) δ 25.4 (pH 7.3); MS (ESI) *m/z* 430.2 [M − PHOOH]$^+$, 496.2 [M + H]$^+$, 518.2 [M + Na]$^+$, 991.1 [2M + H]$^+$, 1013 [2M + Na]$^+$, 1029.2 [2M + K]$^+$; RP-HPLC t_R = 10.5 min (10−90% in 30 min); HRMS (ESI) *m/z* calcd for $C_{22}H_{31}N_3O_6P^{32}S$ 496.1671 [M + H]$^+$, found 496.1665.

1-(Phenylsulfonamido)-2-{4-[2-(piperidin-4-yl)ethoxy]-benzamido}ethylphosphonic Acid (2). A mixture of TFA, TIPS, and water [5 mL, 95:2.5:2.5 (v/v/v) TFA/TIPS/H_2O] was added to **17** (24.1 mg, 0.037 mmol) and the mixture stirred at RT for 16 h. Purification by semipreparative RP-HPLC and lyophilization gave **2** (15.0 mg, 0.029 mmol, 79%) as a white solid: ^{1}H NMR (500 MHz, MeOH-d_3, RT) δ 8.47 (br s, 1 H), 8.18 (br s, 1 H), 8.12−8.05 (m, 1 H), 7.84 (d, ^3J = 7.4 Hz, 2 H), 7.70 (d, ^3J = 8.9 Hz, 2 H), 7.49−7.32 (m, 3 H), 6.95 (d, ^3J = 8.9 Hz, 2 H), 4.13 (t, ^3J = 6.0 Hz, 2 H), 3.96−3.85 (m, 1 H), 3.73−3.62 (m, 1 H), 3.55−3.44 (m, 1 H), 3.43−3.35 (m, 2 H), 3.07−2.93 (m, 2 H), 2.08−1.99 (m, 2 H), 1.98−1.87 (m, 1 H), 1.82 (dd, ^3J = 12.4 Hz, ^3J = 6.1 Hz, 2 H), 1.51 (m, 2 H); ^{13}C NMR (126 MHz, D_2O/CD_3CN/NaOH, RT) δ 167.7, 160.9, 141.4, 131.5, 128.6, 128.5, 125.6, 125.2, 113.7, 65.5, 52.1 (d, ^1J = 134 Hz), 44.8, 41.5 (d, ^2J = 5 Hz), 35.1, 32.1, 31.8; ^{31}P NMR (101 MHz, D_2O/H_2O, RT) δ 13.7 (pH 7.2); MS (EI) *m/z* 430.1 [M − $PO(OH)_2$]$^+$, 494.3 [M − OH]$^+$, 512.2 [M + H]$^+$, 1023.1 [2M + H]$^+$, 1045.1 [2M + Na]$^+$; RP-HPLC t_R = 10.2 min (10−90% in 30 min); HRMS (ESI) *m/z* calcd for $C_{22}H_{31}N_3O_7P^{32}S$ 512.1615 [M + H]$^+$, found 512.1616.

Methyl-1-(phenylsulfonamido)-2-{4-[2-(piperidin-4-yl)-ethoxy]benzamido}ethylphosphonate (3). A mixture of TFA, TIPS, and water [5 mL, 95:2.5:2.5 (v/v/v) TFA/TIPS/H_2O] was added to **18** (16.7 mg, 0.025 mmol) and the mixture stirred at RT for 16 h. Purification by semipreparative RP-HPLC and lyophilization gave **3** (10.4 mg, 0.020 mmol, 78%) as a white solid: ^{1}H NMR (500 MHz, MeOH-d_3, RT) δ 8.60−8.40 (m, 1 H), 8.18 (t, ^3J = 5.2 Hz, 1 H), 7.88 (d, ^3J = 8.0 Hz, 2 H), 7.74 (d, ^3J = 9.0 Hz, 2 H), 7.49 (t, ^3J = 7.2 Hz, 1 H), 7.44 (t, ^3J = 7.5 Hz, 2 H), 7.18−7.11 (m, 1 H), 6.95 (d, ^3J = 9.0 Hz, 2 H), 4.11 (t, ^3J = 6.2 Hz, 2 H), 3.73 (ddd, ^3J = 16.8 Hz, ^3J = 13.3 Hz, ^3J = 8.1 Hz, 1 H), 3.65 (ddd, ^2J = 19.2 Hz, ^3J = 9.8 Hz, ^3J = 4.9 Hz, 1 H), 3.53−3.49 (m, 1 H), 3.42−3.35 (m, 2 H), 3.35 (d, ^3J = 10.5 Hz, 3 H), 3.06−2.32 (m, 2 H), 2.06−1.97 (m, 2 H), 1.97−1.86 (m, 1 H), 1.80 (dt, ^3J = 6.5 Hz, ^3J = 6.3 Hz, 2 H), 1.52−1.39 (m, 2 H); ^{13}C NMR (126 MHz, MeOH-d_3, RT) δ 169.7, 163.1, 142.9, 133.5, 130.3, 130.1, 128.1, 127.7, 115.2, 66.5, 52.7 (d, ^2J = 6.3 Hz), 50.9 (d, ^1J = 147.1 Hz), 45.5, 42.4 (d, ^2J = 6.1 Hz), 36.2, 32.4, 30.1; ^{31}P NMR (101 MHz, D_2O/H_2O, RT) δ 17.6 (pH 6.91); MS (ESI) *m/z* 494.2 [M − OMe]$^+$, 526.2 [M + H]$^+$, 548.2 [M + Na]$^+$, 1051.1 [2M + H]$^+$, 1073.1 [2M + Na]$^+$, 1576.0 [3M + H]$^+$; RP-HPLC t_R = 10.8 min (10−90% in 30 min); HRMS (ESI) *m/z* calcd for $C_{23}H_{33}N_3O_7P^{32}S$ 526.1777 [M + H]$^+$, found 526.1769.

1-(Phenylsulfonamido)-2-{4-[2-(piperidin-4-yl)ethoxy]-benzamido}ethylthiophosphonic Acid (4). *N,O*-Bis-(trimethylsilyl)acetamide (BSA, 18.6 μL, 0.076 mmol) was added to a mixture of **1** (9.60 mg, 0.019 mmol) and sulfur powder (1.86 mg, 0.058 mmol) in DCM (dry, 5 mL) at 0 °C under an argon atmosphere.[34] The mixture was allowed to warm to RT and stirred for 1 h. Concentration in vacuo and purification by semipreparative RP-HPLC gave **4** (7.34 mg, 0.014 mmol, 72%) as a white solid: ^{1}H NMR (500 MHz, MeOD-d_4, RT) δ 7.87 (d, ^3J = 7.8 Hz, 2 H), 7.75 (d, ^3J = 8.6 Hz, 2 H), 7.46 (dd, ^3J = 8.9 Hz, ^3J = 15.9 Hz, 1 H), 7.42 (t, ^3J = 7.4 Hz, 2 H), 6.96 (d, ^3J = 8.6 Hz, 2 H), 4.13 (t, ^3J = 6.0 Hz, 2 H), 3.80 (dt, ^3J = 11.4 Hz, ^3J = 4.5 Hz, 2 H), 3.65−3.56 (m, 1 H), 3.42−3.36 (m, 2 H), 3.04−2.95 (m, 2 H), 2.07−1.99 (m, 2 H), 1.98−1.87 (m, 1 H), 1.85−1.79 (m, 1 H), 1.53−1.42 (m, 2 H); ^{13}C NMR (126 MHz, MeOD-d_4, RT) δ 169.7, 163.1, 142.6, 133.4, 130.3, 129.9, 128.2, 127.7, 115.1, 66.5, 56.8 (d, ^1J = 114.7 Hz), 45.3, 42.3 (d, ^2J = 11.3 Hz), 36.2, 32.3, 30.0; ^{31}P NMR (101 MHz, D_2O/H_2O, RT) δ 51.8 (pH 6.73); MS (ESI) *m/z* 494.2 [M − 2OH]$^+$, 510.2 [M − OH]$^+$, 528.1 [M + H]$^+$, 550.2 [M + Na]$^+$, 1055.0 [2M + H]$^+$; RP-HPLC t_R = 19.1 min (10−50% in 30 min); HRMS (ESI) *m/z* calcd for $C_{22}H_{31}N_3O_6P^{32}S_2$ 528.1392 [M + H]$^+$, found 528.1374.

(9*H*-Fluoren-9-yl)methyl (2-Hydroxyethyl)carbamate (7). 9-Fluorenylmethoxycarbonyl chloride (Fmoc-Cl, 1.55 g, 6.00 mmol) was added to a solution of 2-aminoethanol (0.330 g, 5.40 mmol) in 10% aqueous Na_2CO_3 (50 mL) and the mixture stirred for 2 h at RT. The reaction mixture was extracted with ethyl acetate (3 × 50 mL). The organic phases were combined, washed with aqueous HCl (1 M, 2 × 50 mL) and brine (1 × 50 mL), and dried over $MgSO_4$. Concentration in vacuo and purification by column chromatography (silica gel, 5:1 ethyl acetate/hexane) gave **7** as a white solid (1.48 g, 5.22 mmol, 97%): TLC R_f = 0.5 (5:1 ethyl acetate/hexane) (UV). ^{1}H NMR and ^{13}C NMR spectra were identical to those previously reported.[45]

(9*H*-Fluoren-9-yl)methyl (2-Oxoethyl)carbamate (8). IBX (7.78 g, 27.8 mmol) was added to a solution of **7** (6.06 g, 21.4 mmol) in DMSO (20 mL) and the mixture stirred at RT for 16 h.[17] DCM (1 L) was added to the reaction mixture, and the resulting white

dx.doi.org/10.1021/jm2013826 | J. Med. Chem. 2012, 55, 871−882

suspension was stirred for 0.5 h, prior to filtration through Celite. The organic layer was washed with aqueous saturated Na_2CO_3 (3 × 300 mL) and brine (2 × 300 mL). Each extraction was followed by filtration through Celite, if necessary. Drying over $MgSO_4$ and concentration in vacuo resulted in a yellow crude product, which was purified by column chromatography (silica gel, 5:1 ethyl acetate/hexane) to give **8** (4.81 g, 17.1 mmol, 80%) as a white solid: TLC R_f = 0.8 (5:1 ethyl acetate/hexane) (UV). ^{1}H NMR and ^{13}C NMR spectra were identical to those previously reported.[45]

(9*H*-Fluoren-9-yl)methyl [2-(Hydroxyimino)ethyl]carbamate (9). DIEA (15.3 mL, 89.7 mmol) was added to a mixture of **8** (4.21 g, 15.0 mmol) and hydroxylammonium chloride (3.12 g, 44.9 mmol) in DCM (dry, 40 mL) and the mixture stirred at RT for 16 h.[18] Concentration in vacuo and purification by column chromatography (silica gel, 3:1 ethyl acetate/hexane) gave **9** (2.45 g, 8.27 mmol, 55%) as a slightly yellow colored solid.

2-{*N*-[(9*H*-Fluoren-9-yl)methoxy]carbonylamino}-1-aminoethylphosphinic Acid (10). Commercial 60 wt % aqueous phosphinic acid (40.0 g, 364 mmol) was lyophilized to obtain anhydrous crystalline H_3PO_2, which was subsequently added to a solution of **9** (2.10 g, 7.09 mmol) in methanol (dry, 100 mL). The reaction mixture was heated to reflux for 4 h and then concentrated in vacuo.[18,19] The residue was dissolved in aqueous HCl (3 M, 200 mL) and washed with diethyl ether (3 × 100 mL). The pH was adjusted to 1.5 by addition of solid Na_2CO_3. The resulting precipitate was isolated and purified by RP-HPLC to give **10** (1.25 g, 3.61 mmol, 51%) as a colorless solid.

2-{*N*-[(9*H*-Fluoren-9-yl)methoxy]carbonylamino}-1-(phenylsulfonamido)ethylphosphinic Acid (11). Benzenesulfonyl chloride (0.507 mL, 3.97 mmol) was added to a solution of **10** (0.310 g, 0.895 mmol) in dioxane and aqueous Na_2CO_3 [50 mL, 1:1 dioxane/aqueous Na_2CO_3 (10 wt %)] and stirred at RT for 3 h. The solvent was removed in vacuo and the residue dissolved in water (100 mL). The aqueous phase was acidified (pH 1) by addition of aqueous HCl (3 M) and extracted with ethyl acetate (3 × 50 mL). The combined organic phases were washed with brine (3 × 50 mL) and dried over Na_2SO_4. Concentration in vacuo and lyophilization from dioxane gave **11** (0.382 g, 0.785 mmol, 88%) as a white solid.

2-Amino-1-(phenylsulfonamido)ethylphosphinic Acid (12). A solution of piperidine (20%) in DMF (v/v, 50 mL) was added to **11** (0.672 g, 1.38 mmol) and the mixture stirred at RT for 2 h. Concentration in vacuo and purification by RP-HPLC and lyophilization gave **12** (0.253 g, 0.96 mmol, 69%) as a white solid.

2-[*N*-(Benzyloxycarbonyl)piperidin-4-yl]ethanol (13). Benzyl chloroformate (Cbz-Cl, 6.05 mL, 42.38 mmol) was added to a solution of 2-(piperidin-4-yl)ethanol (5.00 g, 38.7 mmol) in a dioxane/aqueous 10% Na_2CO_3 mixture (1:1, 250 mL) and the mixture stirred at RT for 1 h. The reaction mixture was concentrated in vacuo and the residue dissolved with ethyl acetate (100 mL). The organic phase was washed with aqueous saturated $NaHCO_3$ (2 × 50 mL), aqueous HCl (1 M, 2 × 50 mL), and brine (1 × 50 mL). Drying over $MgSO_4$ was followed by column chromatography (silica gel, 5:1 ethyl acetate/hexane) to give **13** (7.46 g, 28.2 mmol, 73%) as a colorless liquid.

Methyl 4-[2-*N*-(Benzyloxycarbonyl)piperidin-4-ylethyloxy]-benzoate (14). **13** (1.17 g, 4.43 mmol) was added to a solution of methyl 4-hydroxybenzoate (0.62 g, 4.08 mmol) and tributylphosphine (1.31 mL, 5.25 mmol) in THF (dry, 40 mL) at 0 °C under an argon atmosphere. A solution of 1,1-(azodicarbonyl)dipiperidine (ADDP, 1.32 g, 5.23 mmol) in THF (dry, 15 mL) was added within 5 h by the help of a syringe pump, and the reaction mixture was stirred at RT for 16 h.[20,21] The white precipitate was removed by filtration and destroyed. The filtrate was concentrated in vacuo and the residue dissolved in ethyl acetate (100 mL). The organic phase was washed with saturated aqueous Na_2CO_3 (3 × 50 mL), dried over $MgSO_4$, and concentrated in vacuo. Purification by column chromatography (silica gel, 1:2 ethyl acetate/hexane) and crystallization from methanol gave **14** (1.39 g, 3.50 mmol, 86%) as a white solid.[15]

4-[2-*N*-(Benzyloxycarbonyl)piperidin-4-ylethyloxy]benzoic Acid (15). Aqueous NaOH (1 M, 100 mL) was added to a solution of **14** (0.50 g, 1.26 mmol) in ethanol (100 mL) and stirred at RT for 16 h. The reaction mixture was concentrated in vacuo, and the residue was dissolved in water (100 mL) and acidified (pH 1) with HCl (12 M, 10 mL). A white precipitate formed, which was extracted with ethyl acetate (3 × 100 mL). The combined organic phases were washed with brine (1 × 100 mL) and dried over $MgSO_4$. Concentration in vacuo and lyophilization from dioxane gave **15** (0.47 g, 1.23 mmol, 97%) as a white solid.[15]

2-({4-[2-*N*-(Benzyloxycarbonyl)piperidin-4-yl]ethoxy}-benzamido)-1-(phenylsulfonamido)ethylphosphinic Acid (16). HATU (168 mg, 0.442 mmol), **15** (170 mg, 0.443 mmol), and DIEA (452 μL, 2.66 mmol) were dissolved in DMF (dry, 10 mL), and the mixture was stirred at RT for 15 min. A solution of **12** (117 mg, 0.443 mmol) in DMF (dry, 3 mL) was added and the mixture stirred at RT for 16 h. Concentration in vacuo and purification by RP-HPLC gave **16** (234 mg, 0.372 mmol, 84%) as a white solid.

2-({4-[2-*N*-(Benzyloxycarbonyl)piperidin-4-yl]ethoxy}-benzamido)-1-(phenylsulfonamido)ethylphosphonic Acid (17). *N*,*O*-Bis(trimethylsilyl)acetamide (BSA, 98 μL, 0.400 mmol) was added to a solution of **16** (10.1 mg, 0.016 mmol) in DCM (5 mL) and the mixture stirred at RT for 1 h under an ambient atmosphere. Concentration in vacuo, purification by semipreparative HPLC, and lyophilization gave **17** (9.68 mg, 0.015 mmol, 93%) as a white solid.

Methyl 2-(4-{2-[1-(Benzyloxycarbonyl)piperidin-4-yl]-ethoxy}benzamido)-1-(phenylsulfonamido)ethylphosphonate (18). EDC·HCl (25.8 mg, 0.134 mmol) and DMAP (8.3 mg, 0.068 mmol) were added to a solution of **17** (21.7 mg, 0.034 mmol) in methanol (dry, 5 mL), and the mixture was stirred at RT for 2 h. Concentration in vacuo and purification via semipreparative RP-HPLC gave **18** (17.4 mg, 0.026 mmol, 78%) as a white solid.

Integrin Binding Assay (Fibrinogen–αIIbβ3 Assay). The inhibiting activity of the integrin antagonists was determined in a solid-phase binding assay using coated extracellular matrix protein fibrinogen and soluble αIIbβ3 integrin.[26] The assay was based on a previously reported method with some modifications.[27] Flat-bottom 96-well ELISA plates (BRAND, Wertheim, Germany) were coated overnight at 4 °C with 100 μL of 10 μg/mL fibrinogen per well (Calbiochem, Darmstadt, Germany) in carbonate buffer [15 mM Na_2CO_3 and 35 mM $NaHCO_3$ (pH 9.6)]. Wells were then washed three times with PBST buffer [137 mM NaCl, 2.7 mM KCl, 10 mM Na_2HPO_4, 2 mM KH_2PO_4, and 0.01% Tween 20 (pH 7.4)] and blocked for 1 h at room temperature with 150 μL of TSB buffer [20 mM Tris-HCl, 150 mM NaCl, 1 mM $CaCl_2$, 1 mM $MgCl_2$, 1 mM $MnCl_2$ (pH 7.5), and 1% BSA] per well. After being washed three times with PBST, equal amounts of controls (tirofiban, Sigma-Aldrich) or test compounds were mixed with 5.0 μg/mL human integrin αIIbβ3 (Enzyme Research Laboratory, Swansea, U.K.), resulting in a final TSB buffer dilution of 0.00013 to 10 μM for the inhibitors and 2.5 μg/mL for integrin αIIbβ3; 100 μL of these solutions was incubated per well for 1 h at room temperature. The plate was washed three times with PBST buffer, and 100 μL of 2.0 μg/mL primary antibody (mouse anti-human CD41b, BD Biosciences, Heidelberg, Germany) per well was added to the plate. After incubation for 1 h at room temperature, the plate was washed three times with PBST, and 100 μL of 1.0 μg/mL secondary peroxidase-labeled antibody (anti-mouse IgG-POD, Sigma-Aldrich) per well was added to the plate and the plate incubated for 1 h at room temperature. After the plate had been washed three times with PBST, the plate was developed by addition of 50 μL of SeramunBlau fast (Seramun Diagnostic GmbH, Heidesee, Germany) per well and incubated for 5 min at room temperature. The reaction was stopped with 50 μL of 3 M H_2SO_4 per well, and the absorbance was measured at 450 nm with a plate reader (POLARstar Galaxy, BMG Labtechnologies). Each compound concentration was tested in duplicate, and the resulting inhibition curves were analyzed using OriginPro version 7.5G; the inflection point describes the IC_{50} value. Each plate contained tirofiban as an internal control.

In Vitro Permeability Study (Caco-2 test). *Growth and Maintenance of Cells.* Caco-2 cells were obtained from ATCC (Manassas, VA) and then grown in 75 cm^2 flasks with approximately 0.5 × 10^6 cells/flask at 37 °C in a 5% CO_2 atmosphere at a relative humidity of 95%. The culture growth medium consisted of Dulbecco's modified Eagle's medium (DMEM) supplemented with 10% heat-

dx.doi.org/10.1021/jm2013826 | J. Med. Chem. 2012, 55, 871–882

inactivated fetal bovine serum (FBS), 1% nonessential amino acids, 2 mM L-glutamine, 2 mM sodium pyruvate, and a 2 mM penicillin/streptomycin solution.

Preparation of Cells. For transport studies, cells in a passage range of 52−60 were seeded at a density of 25×10^5 cells/cm^2 on untreated culture inserts of a polycarbonate membrane with 0.4 μm pores and a surface area of 1.1 cm^2. The culture inserts containing the Caco-2 monolayer were placed in 24 transwell plates (12 mm, Costar). The culture medium was changed every other day. Transport studies were performed 21−23 days after seeding, when the cells were fully differentiated and the TEER values were stable (300−500 Ω cm^2).

Caco-2 Assay. The transport study (apical to basolateral, A to B) was initiated by removal of medium from both sides of the monolayer and replacement with apical buffer (600 μL) and basolateral buffer (1500 μL), both warmed to 37 °C. The cells were incubated for 30 min at 37 °C with shaking (100 cycles/min). After the incubation period, the buffers were removed and replaced with 1500 μL of basolateral buffer at the basolateral side. Test solutions were preheated to 37 °C and added (600 μL) to the apical side of the monolayer; 50 μL samples were taken from the apical side immediately at the beginning of the experiment, resulting in an apical volume of 550 μL during the experiment. For the period of the experiment, cells were kept at 37 °C with shaking. At predetermined times (30, 60, 90, 120, and 150 min), 200 μL samples were taken from the basolateral side and replaced with the same volume of fresh basolateral buffer to maintain a constant volume. A mass balance was performed for each tested compound to detect instability and/or nonspecific binding of the peptides. For the basolateral to apical study (B to A), compounds were placed in the basolateral chamber, followed by sampling of the apical side, in the same manner used for the A to B protocol.

Blood Samples. Venous blood was collected from a healthy volunteer who had refrained from taking any medication affecting platelet function for the two preceding weeks. Blood was drawn by peripheral venipuncture into 4.5 mL plastic tubes containing recombinant hirudin as an anticoagulant (specified final concentration of 25 μg/mL of blood). Measurements were performed 0.5−4 h after venipuncture.

Platelet Aggregation Assay. Platelet aggregation in hirudin-anticoagulated whole blood with thrombin receptor-activating peptide (TRAP-6, final concentration of 33 μM) as an activator was measured using an impedance-based multiple-electrode platelet aggregometer (Multiplate, Dynabyte Informationssysteme GmbH, Munich, Germany)[28,29] according to the manufacturer's instructions, i.e., at 37 °C, minicuvettes with 175 μL of blood, 175 μL of isotonic saline, and 12 μL of TRAP-6 reagent (1 mM). The only modification was the use of a serial saline dilution of integrin inhibitors instead of pure saline. The increase in electrical impedance was recorded for 6 min and transformed into arbitrary aggregation units, and the area under the curve (AUC) was calculated. Reported AUC values represent the average from two electrode pairs per cuvette. Inhibition curves were analyzed using OriginPro version 7.5G; the inflection point indicates the half-maximal effective concentration (EC_{50}).

Protonation State Calculations. The estimation of pK_a values of compounds **1**−**4** was conducted using the calculator plugin Marvin 5.3, 2010, from ChemAxon (http://www.chemaxon.com). The estimation is computed through an algorithm that uses the empirically calculated atomic charges for each protonation state of a subset of molecules.[46] Each atom of the query molecule is identified in one of the atom's subsets, and via the algorithm, the pK_a is finally calculated. The concentration of the different microspecies formed by a molecule at a given pH is predicted using the distribution coefficient (D), calculated using the previously computed pK_a values.[47]

Molecular Electrostatic Potential Calculations. For tirofiban (**6**) and compounds **1**−**4**, the electrostatic potential was calculated by means of Gaussian03 and mapped onto the electron density surface for each compound. The isovalue of 0.0004 electron/Bhor^3 was chosen for the definition of the density surface, while the electrostatic potential was computed at the Hartree−Fock level of theory using the 6-31G* basis set with a scale of −294.178 (red) to 294.178 (blue) K_bT/e_c. The electrostatic potential of the αIIbβ3 receptor was calculated using the parm99 Amber force field[48,49] through apbs, which is an adaptive Poisson−Boltzmann solver.[50]

Docking Simulations. *Redocking Experiment.* The reliability of AutoDock for this system was assessed through the redocking of the αIIbβ3 cocrystallized ligand, tirofiban (PDB entry 2vdm). The X-ray binding conformation of tirofiban has been clearly predicted by AutoDock among the poses with the best scoring function values (Figure 3A). One may notice that for tirofiban the (*S*)-enantiomer is the bioactive one, while for the phosphorus-containing compounds, because of the change in priority according to the Cahn−Ingold−Prelog rules, the (*R*)-enantiomers are the bioactive ones. Molecular docking calculations for tirofiban and compounds **1**−**4** were conducted using the three-dimensional X-ray structure of αIIbβ3 in the apo form (PDB entry 2vdm) through AutoDock (version 4.0).[36,37] The apo form of αIIbβ3 was obtained via removal of tirofiban from the X-ray complex.

Ligand Setup. The structures of the inhibitors were first generated using the PRODRG server.[51] Then the ligands and the protein were charged using the Gasteiger partial charge[52] and converted to AutoDock format files using AutoDockTools (ADT 1.5.4).

Docking Setup. The docking area was defined by a box, centered approximately on the center of mass of tirofiban cocrystallized with the protein. Grid points (60 × 60 × 60) with 0.375 Å spacing were calculated around the docking area for all the ligand atom types using AutoGrid4. For each ligand, 100 separate docking calculations were performed. Each docking calculation consisted of 2.5×10^6 energy evaluations using the Lamarckian genetic algorithm local search (GALS) method. Otherwise, default docking parameters were applied. The docking conformations were clustered on the basis of the root-mean-square deviation (rmsd of 2 Å) calculated for the Cartesian coordinates of the ligand atoms and then were ranked on the basis of AutoDock scoring function. The binding mode figures were generated using PyMOL (http://www.pymol.org), while the molecular electrostatic potential surfaces were rendered using GaussView.

■ ASSOCIATED CONTENT

Supporting Information

Analytical data of compounds **7**−**18**, HPLC enantiomer separation, ^{31}P NMR titration of compounds **1**−**4**, docking of molecular probes (*R*)-**3** and (*R*)-**4**, docking of (*S*)-enantiomers, and supporting figures. This material is available free of charge via the Internet at http://pubs.acs.org.

■ AUTHOR INFORMATION

Corresponding Author

*Institute for Advanced Study and Center of Integrated Protein Science, Department Chemie, Technische Universität München, Lichtenbergstrasse 4, 85747 Garching, Germany. Phone: +49 (0) 89 289 13300. Fax: +49 (0) 89 289 13210. E-mail: kessler@tum.de.

■ ACKNOWLEDGMENTS

We gratefully acknowledge financial support from the International Graduate School of Science and Engineering (IGSSE) and from the Studienstiftung des deutschen Volkes, Werner Spahl for recording high-resolution mass spectra, Renate Reher for performing the platelet aggregation measurements, and Timo Huber for initial support.

■ ABBREVIATIONS

ADAMs, disintegrin and metalloprotease; AUC, area under the curve; CIP, Cahn−Ingold−Prelog; DMAP, 4-(dimethylamino)-pyridine; ECM, extracellular matrix; EDC, *N*-[3-(dimethylamino)propyl]-*N*′-ethylcarbodiimide; ELISA, enzyme-linked immunosorbent assay; FMD, foot-and-mouth disease; HATU, *O*-(7-azabenzotriazol-1-yl)-*N*,*N*,*N*′,*N*′-tetrame-

thyluronium hexafluorophosphate; IBX, *o*-iodoxybenzoic acid; MIDAS, metal ion-dependent adhesion site; RGD, arginine-glycine-aspartic acid

REFERENCES

(1) Meyer, A.; Auernheimer, J.; Modlinger, A.; Kessler, H. Targeting RGD recognizing integrins: Drug development, biomaterial research, tumor imaging and targeting. *Curr. Pharm. Des.* **2006**, *12*, 2723−2747.

(2) Mousa, S. A. Anti-integrin as novel drug-discovery targets: Potential therapeutic and diagnostic implications. *Curr. Opin. Chem. Biol.* **2002**, *6*, 534−541.

(3) Humphries, M. J. Integrin structure. *Biochem. Soc. Trans.* **2000**, *28*, 311−339.

(4) Arnaout, M. A.; Mahalingam, B.; Xiong, J. P. Integrin structure, allostery, and bidirectional signaling. *Annu. Rev. Cell Dev. Biol.* **2005**, *21*, 381−410.

(5) Hynes, R. O. Integrins: Bidirectional, allosteric signaling machines. *Cell* **2002**, *110*, 673−687.

(6) Humphries, J. D.; Byron, A.; Humphries, M. J. Integrin ligands at a glance. *J. Cell Sci.* **2006**, *119*, 3901−3903.

(7) Ruoslahti, E. RGD and other recognition sequences for integrins. *Annu. Rev. Cell Dev. Biol.* **1996**, *12*, 697−715.

(8) Heckmann, D.; Laufer, B.; Marinelli, L.; Limongelli, V.; Novellino, E.; Zahn, G.; Stragies, R.; Kessler, H. Breaking the dogma of the metal-coordinating carboxylate group in integrin ligands: Introducing hydroxamic acids to the MIDAS to tune potency and selectivity. *Angew. Chem., Int. Ed.* **2009**, *48*, 4436−4440.

(9) Cox, D.; Brennan, M.; Moran, N. Integrins as therapeutic targets: Lessons and opportunities. *Nat. Rev. Drug Discovery* **2010**, *9*, 804−820.

(10) Mas-Moruno, C.; Rechenmacher, F.; Kessler, H. Cilengitide: The first anti-angiogenic small molecule drug candidate. Design, synthesis and clinical evaluation. *Anti-Cancer Agents Med. Chem.* **2011**, *10*, 753−768.

(11) Shimaoka, M.; Springer, T. A. Therapeutic antagonists and conformational regulation of integrin function. *Nat. Rev. Drug Discovery* **2003**, *2*, 703−716.

(12) Hartman, G. D.; Egbertson, M. S.; Halczenko, W.; Laswell, W. L.; Duggan, M. E.; Smith, R. L.; Naylor, A. M.; Manno, P. D.; Lynch, R. J.; Zhang, G.; Chang, C. T.-C.; Gould, R. J. Non-peptide fibrinogen receptor antagonists. 1. Discovery and design of exosite inhibitors. *J. Med. Chem.* **1992**, *35*, 4640−4642.

(13) Topol, E. J.; Moliterno, D. J.; Herrmann, H. C.; Powers, E. R.; Grines, C. L.; Cohen, D. J.; Cohen, E. A.; Bertrand, M.; Neumann, F. J.; Stone, G. W.; DiBattiste, P. M.; Demopoulos, L. Comparison of two platelet glycoprotein IIb/IIIa inhibitors, tirofiban and abciximab, for the prevention of ischemic events with percutaneous coronary revascularization. *N. Engl. J. Med.* **2001**, *344*, 1888−1894.

(14) Cannon, C. P.; Weintraub, W. S.; Demopoulos, L. A.; Vicari, R.; Frey, M. J.; Lakkis, N.; Neumann, F. J.; Robertson, D. H.; DeLucca, P. T.; DiBattiste, P. M.; Gibson, C. M.; Braunwald, E. Comparison of early invasive and conservative strategies in patients with unstable coronary syndromes treated with the glycoprotein IIb/IIIa inhibitor tirofiban. *N. Engl. J. Med.* **2001**, *344*, 1879−1887.

(15) Duggan, M. E.; Duong, L. T.; Fisher, J. E.; Hamill, T. G.; Hoffman, W. F.; Huff, J. R.; Ihle, N. C.; Leu, C. T.; Nagy, R. M.; Perkins, J. J.; Rodan, S. B.; Wesolowski, G.; Whitman, D. B.; Zartman, A. E.; Rodan, G. A.; Hartman, G. D. Nonpeptide $\alpha_v\beta_3$ antagonists. 1. Transformation of a potent, integrin-selective $\alpha_{IIb}\beta_3$ antagonist into a potent $\alpha_v\beta_3$ antagonist. *J. Med. Chem.* **2000**, *43*, 3736−3745.

(16) Frigerio, M.; Santagostino, M.; Sputore, S. A user-friendly entry to 2-iodoxybenzoic acid (IBX). *J. Org. Chem.* **1999**, *64*, 4537−4538.

(17) Frigerio, M.; Santagostino, M. A mild oxidizing reagent for alcohols and 1,2-diols: o-Iodoxybenzoic acid (IBX) in DMSO. *Tetrahedron Lett.* **1994**, *35*, 8019−8022.

(18) Liboska, R.; Pícha, J.; Hanclová, I.; Budesínský, M.; Sanda, M.; Jirácek, J. Synthesis of methionine- and norleucine-derived phosphinopeptides. *Tetrahedron Lett.* **2008**, *49*, 5629−5631.

(19) Zhukov, Y. N.; Khomutov, A. R.; Osipova, T. I.; Khomutov, R. M. Synthesis of phosphinic analogs of sulfur-containing amino acids. *Russ. Chem. Bull.* **1999**, *48*, 1348−1351.

(20) Heckmann, D.; Meyer, A.; Laufer, B.; Zahn, G.; Stragies, R.; Kessler, H. Rational design of highly active and selective ligands for the $\alpha5\beta1$ integrin receptor. *ChemBioChem* **2008**, *9*, 1397−1407.

(21) Marugán, J. J.; Manthey, C.; Anaclerio, B.; Lafrance, L.; Lu, T.; Markotan, T.; Leonard, K. A.; Crysler, C.; Eisennagel, S.; Dasgupta, M.; Tomczuk, B. Design, synthesis, and biological evaluation of novel potent and selective $\alpha_v\beta_3/\alpha_v\beta_5$ integrin dual inhibitors with improved bioavailability. Selection of the molecular core. *J. Med. Chem.* **2005**, *48*, 926−934.

(22) Hoffmann, C. V.; Pell, R.; Lämmerhofer, M.; Lindner, W. Synergistic effects on enantioselectivity of zwitterionic chiral stationary phases for separations of chiral acids, bases, and amino acids by HPLC. *Anal. Chem.* **2008**, *80*, 8780−8789.

(23) Hoffmann, C. V.; Reischl, R.; Maier, N. M.; Lämmerhofer, M.; Lindner, W. Stationary phase-related investigations of quinine-based zwitterionic chiral stationary phases operated in anion-, cation-, and zwitterion-exchange modes. *J. Chromatogr., A* **2009**, *1216*, 1147−1156.

(24) Maier, N. M.; Schefzick, S.; Lombardo, G. M.; Feliz, M.; Rissanen, K.; Lindner, W.; Lipkowitz, K. B. Elucidation of the chiral recognition mechanism of cinchona alkaloid carbamate-type receptors for 3,5-dinitrobenzoyl amino acids. *J. Am. Chem. Soc.* **2002**, *124*, 8611−8629.

(25) Lämmerhofer, M.; Hebenstreit, D.; Gavioli, E.; Lindner, W.; Mucha, A.; Kafarski, P.; Wieczorek, P. High-performance liquid chromatographic enantiomer separation and determination of absolute configurations of phosphinic acid analogues of dipeptides and their α-aminophosphinic acid precursors. *Tetrahedron: Asymmetry* **2003**, *14*, 2557−2565.

(26) Mas-Moruno, C.; Beck, J. G.; Doedens, L.; Frank, A. O.; Marinelli, L.; Cosconati, S.; Novellino, E.; Kessler, H. Increasing $\alpha v\beta3$ selectivity of the anti-angiogenic drug cilengitide by *N*-methylation. *Angew. Chem., Int. Ed.* **2011**, *50*, 9496−9500.

(27) Chatterjee, J.; Ovadia, O.; Zahn, G.; Marinelli, L.; Hoffman, A.; Gilon, C.; Kessler, H. Multiple N-methylation by a designed approach enhances receptor selectivity. *J. Med. Chem.* **2007**, *50*, 5878−5881.

(28) Tóth, O.; Calatzis, A.; Penz, S.; Losonczy, H.; Siess, W. Multiple electrode aggregometry: A new device to measure platelet aggregation in whole blood. *Thromb. Haemostasis* **2006**, *96*, 781−788.

(29) Halimeh, S.; Angelis, G.; Sander, A.; Edelbusch, C.; Rott, H.; Thedieck, S.; Mesters, R.; Schlegel, N.; Nowak-Gottl, U. Multiplate whole blood impedance point of care aggregometry: Preliminary reference values in healthy infants, children and adolescents. *Klin. Paediatr.* **2010**, *222*, 158−163.

(30) Artursson, P.; Karlsson, J. Correlation between oral drug absorption in humans and apparent drug permeability coefficients in human intestinal epithelial (Caco-2) cells. *Biochem. Biophys. Res. Commun.* **1991**, *175*, 880−885.

(31) Kelley, J. L.; McLean, E. W.; Crouch, R. C.; Averett, D. R.; Tuttle, J. V. [[(Guaninylalkyl)phosphinico]methyl]phosphonic acids. Multisubstrate analogue inhibitors of human erythrocyte purine nucleoside phosphorylase. *J. Med. Chem.* **1995**, *38*, 1005−1014.

(32) Manzenrieder, F.; Frank, A. O.; Kessler, H. Phosphorus NMR spectroscopy as a versatile tool for compound library screening. *Angew. Chem., Int. Ed.* **2008**, *47*, 2608−2611.

(33) Stirtan, W. G.; Withers, S. G. Phosphonate and α-fluorophosphonate analogue probes of the ionization state of pyridoxal 5′-phosphate (PLP) in glycogen phosphorylase. *Biochemistry (Moscow, Russ. Fed.)* **1996**, *35*, 15057−15064.

(34) Selvam, C.; Goudet, C.; Oueslati, N.; Pin, J. P.; Acher, F. C. L-(+)-2-Amino-4-thiophosphonobutyric acid (L-thioAP4), a new potent agonist of group III metabotropic glutamate receptors: Increased distal acidity affords enhanced potency. *J. Med. Chem.* **2007**, *50*, 4656−4664.

(35) Castellino, S.; Leo, G. C.; Sammons, R. D.; Sikorski, J. A. ^{31}P, ^{15}N, and ^{13}C NMR of glyphosate: Comparison of pH titrations to the herbicidal dead-end complex with 5-enolpyruvoylshikimate-3-phos-

phate synthase. *Biochemistry (Moscow, Russ. Fed.)* **1989**, *28*, 3856−3868.
(36) Morris, G. M.; Goodsell, D. S.; Halliday, R. S.; Huey, R.; Hart, W. E.; Belew, R. K.; Olson, A. J. Automated docking using a Lamarckian genetic algorithm and an empirical binding free energy function. *J. Comput. Chem.* **1998**, *19*, 1639−1662.
(37) Huey, R.; Morris, G. M.; Olson, A. J.; Goodsell, D. S. A semiempirical free energy force field with charge-based desolvation. *J. Comput. Chem.* **2007**, *28*, 1145−1152.
(38) Jones, G.; Willett, P.; Glen, R. C.; Leach, A. R.; Taylor, R. Development and validation of a genetic algorithm for flexible docking. *J. Mol. Biol.* **1997**, *267*, 727−748.
(39) Rarey, M.; Kramer, B.; Lengauer, T.; Klebe, G. A fast flexible docking method using an incremental construction algorithm. *J. Mol. Biol.* **1996**, *261*, 470−489.
(40) Gohlke, H.; Hendlich, M.; Klebe, G. Knowledge-based scoring function to predict protein-ligand interactions. *J. Mol. Biol.* **2000**, *295*, 337−356.
(41) Oelschlaeger, P.; Klahn, M.; Beard, W. A.; Wilson, S. H.; Warshel, A. Magnesium-cationic dummy atom molecules enhance representation of DNA polymerase β in molecular dynamics simulations: Improved accuracy in studies of structural features and mutational effects. *J. Mol. Biol.* **2007**, *366*, 687−701.
(42) Rucker, R.; Oelschlaeger, P.; Warshel, A. A binding free energy decomposition approach for accurate calculations of the fidelity of DNA polymerases. *Proteins* **2010**, *78*, 671−680.
(43) Xiang, Y.; Oelschlaeger, P.; Florian, J.; Goodman, M. F.; Warshel, A. Simulating the effect of DNA polymerase mutations on transition-state energetics and fidelity: Evaluating amino acid group contribution and allosteric coupling for ionized residues in human Pol β. *Biochemistry (Moscow, Russ. Fed.)* **2006**, *45*, 7036−7048.
(44) Gottlieb, H. E.; Kotlyar, V.; Nudelman, A. NMR chemical shifts of common laboratory solvents as trace impurities. *J. Org. Chem.* **1997**, *62*, 7512−7515.
(45) Porcheddu, A.; Giacomelli, G.; Piredda, I.; Carta, M.; Nieddu, G. A practical and efficient approach to PNA monomers compatible with Fmoc-mediated solid-phase synthesis protocols. *Eur. J. Org. Chem.* **2008**, *2008*, 5786−5797.
(46) Dixon, S. L.; Jurs, P. C. Estimation of pKa for organic oxyacids using calculated atomic charges. *J. Comput. Chem.* **1993**, *14*, 1460−1467.
(47) Csizmadia, F.; Tsantili-Kakoulidou, A.; Panderi, I.; Darvas, F. Prediction of distribution coefficient from structure. 1. Estimation method. *J. Pharm. Sci.* **1997**, *86*, 865−871.
(48) Cornell, W. D.; Cieplak, P.; Bayly, C. I.; Gould, I. R.; Merz, K. M.; Ferguson, D. M.; Spellmeyer, D. C.; Fox, T.; Caldwell, J. W.; Kollman, P. A. A second generation force field for the simulation of proteins, nucleic acids, and organic molecules. *J. Am. Chem. Soc.* **1995**, *117*, 5179−5197.
(49) Wang, J.; Cieplak, P.; Kollman, P. A. How well does a restrained electrostatic potential (RESP) model perform in calculating conformational energies of organic and biological molecules? *J. Comput. Chem.* **2000**, *21*, 1049−1074.
(50) Baker, N. A.; Sept, D.; Joseph, S.; Holst, M. J.; McCammon, J. A. Electrostatics of nanosystems: Application to microtubules and the ribosome. *Proc. Natl. Acad. Sci. U.S.A.* **2001**, *98*, 10037−10041.
(51) Schüttelkopf, A. W.; van Aalten, D. M. F. PRODRG: A tool for high-throughput crystallography of protein-ligand complexes. *Acta Crystallogr.* **2004**, *D60*, 1355−1363.
(52) Gasteiger, J.; Marsili, M. Iterative partial equalization of orbital electronegativity: A rapid access to atomic charges. *Tetrahedron* **1980**, *36*, 3219−3228.